IEICE TRANS. COMMUN., VOL.E91–B, NO.7 JULY 2008

PAPER

# Coherent Decomposition of Fully Polarimetric FM-CW Radar Data

**Jun NAKAMURA**[†], **Kazuyasu AOYAMA**[†], **Muneyuki IKARASHI**[†], ***Student Members***,
**Yoshio YAMAGUCHI**[††a)], ***Fellow***, ***and*** **Hiroyoshi YAMADA**[††], ***Member***

**SUMMARY** This paper presents a coherent decomposition scheme for polarimetric SAR data. Coherent decomposition means the decomposition is applied to a single or a few scattering matrix data. Based on the scattering matrix acquired with an FM-CW polarimetric SAR system, we have devised a simple decomposition technique using the coherency matrix for the purpose of identifying scatterers. This paper presents the decomposition technique and some decomposition results obtained by a fully polarimetric FM-CW radar. It is shown the scattering mechanisms are well recovered and the orientation angles of wire scatterer are precisely measured.

***key words:*** *coherent decomposition, radar polarimetry, POLSAR, FM-CW radar*

## 1. Introduction

Decomposition of polarimetric scattering nature has been attracting attention in radar remote sensing, for applications of land cover monitoring, detection of environmental change, classification of terrain, etc. [1]–[3].

The decomposition of polarimetric scattering characteristics can be classified into two ways. The first one is based on the statistical characteristics of scatterers. This approach is suitable for vast area decomposition where the scattering objects are large enough compared to radar resolutions such as various terrain areas. It is assumed that enough data are available for obtaining the statistical average [3].

The second approach is used when only a few scattering matrix data are available. This corresponds to a situation of snapshot-like data acquisition scenario. The number of data is not sufficient to ensure statistical evaluations. The statistical scattering nature inherent to scatterer is not available. In this case, it is necessary to carry out coherent decomposition.

E. Krogager has proposed "Ks, Kd, Kh" decomposition scheme based on the scattering matrix in the circular polarization basis [2]. This method decomposes scattering matrix directly and it reveals coherent scattering mechanism. However, it has been pointed out [1] that the decomposition is not based on the orthogonal basis. In addition, the method works well only for metallic objects [4], because the expansion matrices are based on metallic object. It is known that the diffuse or volume scatterings are not well formulated although they exist in the actual phenomena. This paper presents alternative coherent decomposition of scattering mechanism. The advantage of this method is stable for coherent and incoherent data analysis because the scheme is based on the coherency matrix consisting of orthogonal second-order polarimetric moments and power expressions.

In the following, a basis for the coherent four-component decomposition scheme is provided. Then the scheme is applied to FM-CW polarimetric SAR data as well as real aperture radar data. The decomposition results obtained by the radar system are demonstrated to show the effectiveness of the method.

## 2. Coherent Decomposition

The coherency matrix is given as

$$[T] = \boldsymbol{k}_P \boldsymbol{k}_P^{\dagger} \tag{1}$$

where † denotes complex conjugation and transposition, and the Pauli vector $\boldsymbol{k}_P$ is defined as

$$\boldsymbol{k}_P = \frac{1}{\sqrt{2}} \begin{bmatrix} S_{HH} + S_{VV} \\ S_{HH} - S_{VV} \\ 2S_{SV} \end{bmatrix}. \tag{2}$$

We assume monostatic scattering case [1] as defined by (2).

### 2.1 Coherency Matrices of Fundamental Scatterers

To establish the basis function matrix, it is necessary to derive the coherency matrices for the fundamental scatterers (plate, wire, helix, diplane = dihedral corner reflector). Since the scattering matrix $[S(\theta)]$ rotated by angle $\theta$ as shown in Fig. 1 can be expressed as

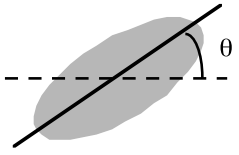


**Fig. 1** Oriented scatterer.

Manuscript received August 6, 2007.
Manuscript revised January 31, 2008.

[†]The authors are with the Graduate School of Science & Technology, Niigata University, Niigata-shi, 950-2181 Japan.
[††]The authors are with the Faculty of Engineering, Niigata University, Niigata-shi, 950-2151 Japan.
a) E-mail: yamaguch@ie.niigata-u.ac.jp

DOI: 10.1093/ietcom/e91–b.7.2374

$$[S(\theta)] = \begin{bmatrix} S_{hh} & S_{hv} \\ S_{hv} & S_{vv} \end{bmatrix} = \begin{bmatrix} \cos\theta & \sin\theta \\ -\sin\theta & \cos\theta \end{bmatrix} \begin{bmatrix} S_{HH} & S_{HV} \\ S_{HV} & S_{VV} \end{bmatrix} \begin{bmatrix} \cos\theta & -\sin\theta \\ \sin\theta & \cos\theta \end{bmatrix} \quad (3)$$

the coherent matrices for these scatterers are derived as shown in Table 1. In order to identify the difference of coherent and averaged cases, both forms are listed in Table 1. The averaged matrices are obtained by integration over orientation angle [0–2$\pi$]. It is seen that the forms of averaged and non-averaged coherency matrix are different for diplane and wire scatterers. Plate and helix have the same forms in the coherent and averaged cases.

Since we are dealing with coherent case, we choose the following matrices for the expansion.

$$\text{Helix: } [T]_{helix} = \frac{1}{2}\begin{bmatrix} 0 & 0 & 0 \\ 0 & 1 & \mp j \\ 0 & \pm j & 1 \end{bmatrix} \quad (4)$$

The sign in front of $j$ in (4) corresponds to Left or Right Helix as seen in Table 1.

$$\text{Plate: } [T]_{plate} = \begin{bmatrix} 1 & 0 & 0 \\ 0 & 0 & 0 \\ 0 & 0 & 0 \end{bmatrix} \quad (5)$$

$$\text{Diplane: } [T]_{diplane} = \begin{bmatrix} 0 & 0 & 0 \\ 0 & \cos^2 2\varphi & -\dfrac{\sin 4\varphi}{2} \\ 0 & -\dfrac{\sin 4\varphi}{2} & \sin^2 2\varphi \end{bmatrix} \quad (6)$$

$$\text{Wire: } [T]_{wire} = \frac{1}{2}\begin{bmatrix} 1 & \cos 2\theta & -\sin 2\theta \\ \cos 2\theta & \cos^2 2\theta & -\dfrac{\sin 4\theta}{2} \\ -\sin 2\theta & -\dfrac{\sin 4\theta}{2} & \sin^2 2\theta \end{bmatrix}, \quad (7)$$

where angles $\varphi$ and $\theta$ are orientation angles with respect to the horizontal direction as seen in Fig. 1. The angle $\varphi$ is assigned to the orientation of diplane in order to distinguish from $\theta$ for wire.

The sum of diagonal elements is "Trace," which also represents the power. The traces of these matrices (4)–(7) are normalized to unity so that the expansion coefficients $P_i$ ($i = c, s, d, w$) represent power contributions which follows.

## 2.2 Decomposition of Coherency Matrix

Assuming that a few scattering matrix data are available, we expand the measured coherency matrix into four submatrices as

$$\langle [T] \rangle^{HV} = \begin{bmatrix} T_{11} & T_{12} & T_{13} \\ T_{21} & T_{22} & T_{23} \\ T_{31} & T_{32} & T_{33} \end{bmatrix} = P_s[T]_{plane} + P_d[T]_{diplane} + P_w[T]_{wire} + P_c[T]_{helix} \quad (8)$$

where $P_s$, $P_d$, $P_w$, $P_c$ are expansion coefficients representing single bounce scattering, double bounce scattering, wire scattering and helix scattering. The symbol $\langle\ \ \rangle$ denotes data averaging of a few pixels. Comparison of the matrix elements leads to the following relations.

$$T_{11}: \ \frac{1}{2}\langle |S_{HH} + S_{VV}|^2 \rangle = P_s + \frac{P_w}{2} \quad (9)$$

$$T_{12} + T_{21}: \ \langle |S_{HH}|^2 - |S_{VV}|^2 \rangle = P_w \cos 2\theta \quad (10)$$

$$T_{13} + T_{31}: \ \mathrm{Re}\langle 2S^*_{HV}(S_{HH} + S_{VV}) \rangle = -P_w \sin 2\theta \quad (11)$$

$$T_{23}: \ \langle S^*_{HV}(S_{HH} - S_{VV}) \rangle = \mp j\frac{P_c}{2} - \frac{P_w}{4}\sin 4\theta - \frac{P_d}{2}\sin 4\varphi \quad (12)$$

**Table 1** Coherency matrix of fundamental scatterer.

| | Scattering matrix $[S(\theta)]$ | Scattering vector $\boldsymbol{k}(\theta)$ | Coherency matrix $[T(\theta)]$ $Trace = 1$ | Averaged Coherency matrix $\langle [T(\theta)] \rangle$ |
|---|---|---|---|---|
| Plate | $\begin{bmatrix} 1 & 0 \\ 0 & 1 \end{bmatrix}$ | $\frac{1}{\sqrt{2}}\begin{bmatrix} 2 \\ 0 \\ 0 \end{bmatrix}$ | $\begin{bmatrix} 1 & 0 & 0 \\ 0 & 0 & 0 \\ 0 & 0 & 0 \end{bmatrix}$ | $\begin{bmatrix} 1 & 0 & 0 \\ 0 & 0 & 0 \\ 0 & 0 & 0 \end{bmatrix}$ |
| Diplane | $\begin{bmatrix} \cos 2\theta & -\sin 2\theta \\ -\sin 2\theta & -\cos 2\theta \end{bmatrix}$ | $\sqrt{2}\begin{bmatrix} 0 \\ \cos 2\theta \\ -\sin 2\theta \end{bmatrix}$ | $\begin{bmatrix} 0 & 0 & 0 \\ 0 & \cos^2 2\theta - \frac{\sin 4\theta}{2} & \\ 0 & -\frac{\sin 4\theta}{2} & \sin^2 2\theta \end{bmatrix}$ | $\frac{1}{2}\begin{bmatrix} 0 & 0 & 0 \\ 0 & 1 & 0 \\ 0 & 0 & 1 \end{bmatrix}$ |
| Dipole, wire | $\begin{bmatrix} \cos^2\theta & -\frac{1}{2}\sin 2\theta \\ -\frac{1}{2}\sin 2\theta & \sin^2\theta \end{bmatrix}$ | $\frac{1}{\sqrt{2}}\begin{bmatrix} 1 \\ \cos 2\theta \\ -\sin 2\theta \end{bmatrix}$ | $\frac{1}{2}\begin{bmatrix} 1 & \cos 2\theta & -\sin 2\theta \\ \cos 2\theta & \cos^2 2\theta - \frac{\sin 4\theta}{2} & \\ -\sin 2\theta & -\frac{\sin 4\theta}{2} & \sin^2 2\theta \end{bmatrix}$ | $\frac{1}{4}\begin{bmatrix} 2 & 0 & 0 \\ 0 & 1 & 0 \\ 0 & 0 & 1 \end{bmatrix}$ |
| Left helix | $\frac{e^{j2\theta}}{2}\begin{bmatrix} 1 & j \\ j & -1 \end{bmatrix}$ | $\frac{e^{j2\theta}}{\sqrt{2}}\begin{bmatrix} 0 \\ 1 \\ j \end{bmatrix}$ | $\frac{1}{2}\begin{bmatrix} 0 & 0 & 0 \\ 0 & 1 & -j \\ 0 & j & 1 \end{bmatrix}$ | $\frac{1}{2}\begin{bmatrix} 0 & 0 & 0 \\ 0 & 1 & -j \\ 0 & j & 1 \end{bmatrix}$ |
| Right helix | $\frac{e^{-j2\theta}}{2}\begin{bmatrix} 1 & -j \\ -j & -1 \end{bmatrix}$ | $\frac{e^{-j2\theta}}{\sqrt{2}}\begin{bmatrix} 0 \\ 1 \\ -j \end{bmatrix}$ | $\frac{1}{2}\begin{bmatrix} 0 & 0 & 0 \\ 0 & 1 & j \\ 0 & -j & 1 \end{bmatrix}$ | $\frac{1}{2}\begin{bmatrix} 0 & 0 & 0 \\ 0 & 1 & j \\ 0 & -j & 1 \end{bmatrix}$ |

$$T_{32}:\ \langle S_{HV}(S_{HH}-S_{VV})^*\rangle = \pm j\frac{P_c}{2} - \frac{P_w}{4}\sin 4\theta - \frac{P_d}{2}\sin 4\varphi \tag{13}$$

$$T_{22}:\ \frac{1}{2}\langle|S_{HH}-S_{VV}|^2\rangle = \frac{P_c}{2} + \frac{P_w}{2}\cos^2 2\theta + P_d\cos^2 2\varphi \tag{14}$$

$$T_{33}:\ \langle 2|S_{HV}|^2\rangle = \frac{P_c}{2} + \frac{P_w}{2}\sin^2 2\theta + P_d\sin^2 2\varphi \tag{15}$$

The expansion coefficients $P_i$ $(i = s, d, w, c)$ and angles $\theta$ can $\varphi$ be determined by (9)–(15) as follows.

From the imaginary part of (13)–(12), helix scattering power $P_c$ can be derived,

$$P_c = |\mathrm{Im}\langle 2S^*_{HV}(S_{HH}-S_{VV})\rangle|, \tag{16}$$

where $\mathrm{Im}\langle S^*_{HV}(S_{HH}-S_{VV})\rangle > 0$ corresponds to Right-helix, and $\mathrm{Im}\langle S^*_{HV}(S_{HH}-S_{VV})\rangle < 0$ corresponds to Left-helix.

The square sum of (10) and (11) yields wire scattering power $P_w$,

$$P_w = \sqrt{\langle|S_{HH}|^2-|S_{VV}|^2\rangle^2 + \mathrm{Re}^2\langle 2S^*_{HV}(S_{HH}+S_{VV})\rangle} \tag{17}$$

It is possible to find wire orientation angle by (10),

$$\theta = \frac{1}{2}\cos^{-1}\left\{\frac{1}{P_w}\langle|S_{HH}|^2 - |S_{VV}|^2\rangle\right\}. \tag{18}$$

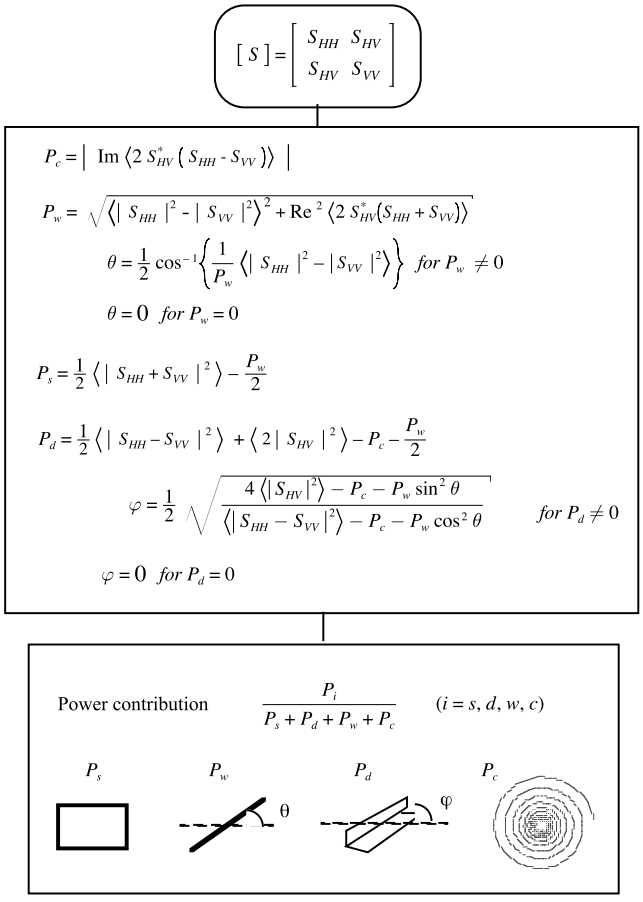


**Fig. 2** Coherent decomposition algorithm.

Single bounce scattering power $P_s$ is determined using $P_w$,

$$P_s = \frac{1}{2}\langle|S_{HH}+S_{VV}|^2\rangle - \frac{P_w}{2}. \tag{19}$$

Finally, double bounce scattering power $P_d$ and the orientation angle are determined by (14) and (15),

$$P_d = \frac{1}{2}\langle|S_{HH}-S_{VV}|^2\rangle + \langle 2|S_{HV}|^2\rangle - P_c - \frac{P_w}{2} \tag{20}$$

$$\varphi = \pm\frac{1}{2}\tan^{-1}\sqrt{\frac{4\langle|S_{HV}|^2\rangle - P_c - P_w\sin^2 2\theta}{\langle|S_{HH}-S_{VV}|^2\rangle - P_c - P_w\cos^2 2\theta}}. \tag{21}$$

Therefore, we can find the scattering powers $P_i$ and the orientation angles directly (16)–(21).

### 2.3 Decomposition Algorithm

The decomposition algorithm based on the above expansion can be expressed as shown in Fig. 2. Once the powers are determined, the ratio of power contribution is used for identifying main the scatterer.

$$\frac{P_i}{P_s + P_d + P_w + P_c} \quad (i = s, d, w, c) \tag{22}$$

The decomposition is quite simple as seen in Fig. 2.

## 3. Laboratory Experiment

### 3.1 FM-CW POLSAR System

A fully polarimetric FM-CW radar system (POLSAR) has been developed for the purpose of laboratory measurements in Niigata University [5]. It is operative in the Ku-band and the X-band.

The flow of the data acquisition is shown in Fig. 3. The PC sends a trigger, and then the saw tooth wave generator and the sweeper make an FM signal. The power splitter divides the signal into transmitting and reference signals. This transmitting signal is radiated by H polarized antenna, and then two orthogonal antennas receive the reflected signals

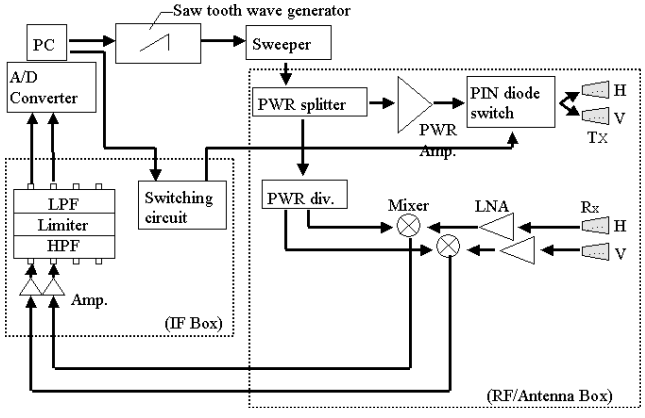


**Fig. 3** Block diagram of the FM-CW POLSAR.

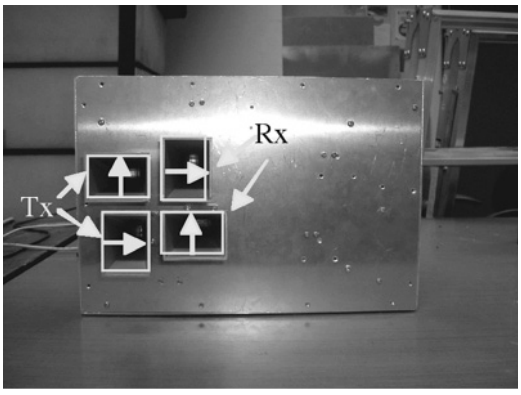


**Fig. 4** FM-CW POLSAR antennas in the Ku-band.

**Table 2** FM-CW POLSAR system.

| | |
|---|---|
| Operating frequency | 9 - 18 GHz |
| Sweep frequency | 2 GHz (default) |
| Sweep time | 5 ms |
| Polarization | HH, HV, VH, VV |
| Range resolution | 7.5 cm (default) |
| Cross talk | Less than - 24 dB |
| Dynamic range | 50 dB |
| Data acquisition time | 20 ms/snapshot |

simultaneously. Each signal is mixed with the reference signal. When one (ex. H polarized case) record is completed, then the PIN diode switch replaces the transmitting antenna, and the same procedure is repeated. Figure 4 shows the polarimetric antenna system of the radar.

The features of the FM-CW POLSAR system are listed in Table 2. The frequency band can be adjusted arbitrary to obtain various range resolution imaging. The X-band frequency (9–11 GHz) was used in the measurement.

### 3.2 Decomposition Result of Fundamental Target

Polarimetric SAR measurement was carried out in anechoic chamber to verify the decomposition result. At first, it is necessary to remove polarimetric error in data acquisition. Polarimetric calibration is indispensable for polarimetric radar operation. We have calibrated acquired scattering matrix data according to the procedure [6]. Figure 5 shows a polarization signature of trihedral corner reflector before and after the polarimetric calibration, indicating the polarimetric data is reliable.

The scatterers used in the measurement and the measurement conditions are listed in Table 3.

Figure 6 shows SAR images of scatterers together with the power contribution ratio in%. Averaging size is 5 in the range direction and 5 in the azimuth direction. It is seen that the decomposition is quite successful.

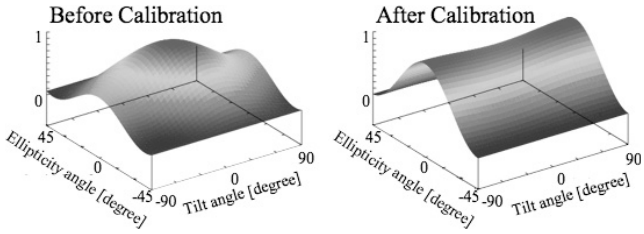


**Fig. 5** Polarization signature before and after calibration for square-sided trihedral corner reflector (10 cm by 10 cm).

**Table 3** Measurement conditions.

| Scatteres | |
|---|---|
| Sphere | 15 cm in diameter |
| Diplane | one plane : 6 x 10 cm |
| Parallel plate waveguide | 6.5 x 10.5 cm |
| Range | 2 m |
| Frequency | 9 - 11 GHz |
| Scan width / pitch | 128 cm / 1 cm |
| Number of FFT points | 16384 |

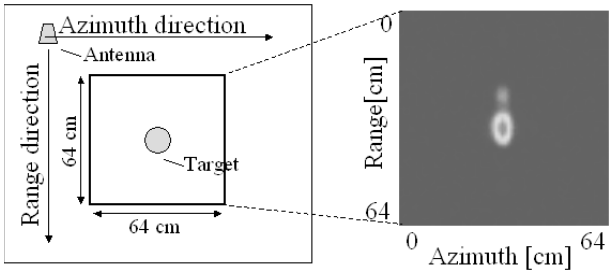


(a) Measurement situation and the corresponding SAR image configuration.

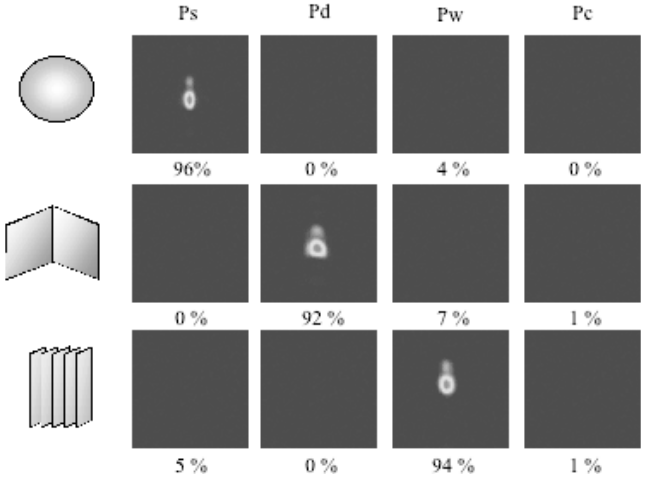


(b) Scatterer and decomposed SAR image.

**Fig. 6** Decomposed result of fundamental scatterer.

### 3.3 Orientation Angle Estimation

Once the scatterer under test is recognized as wire, it is pos-

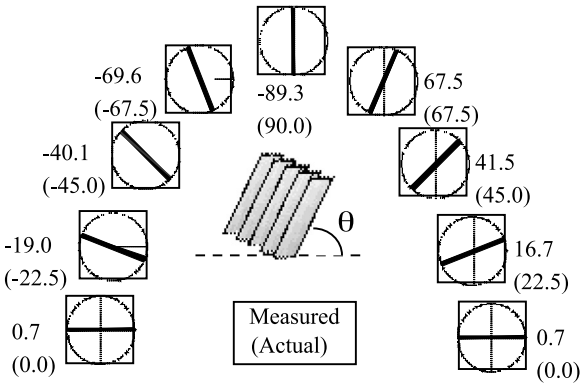


**Fig. 7** Orientation angle detection.

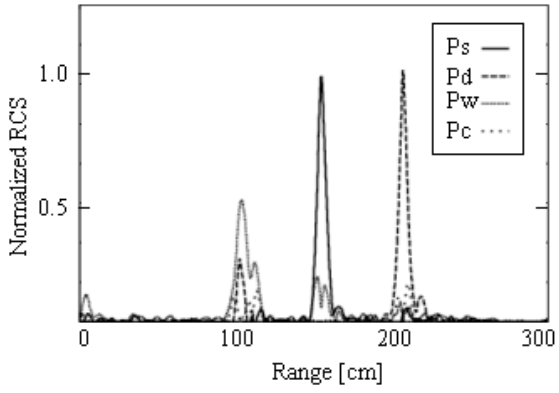


(a) Decomposed result.

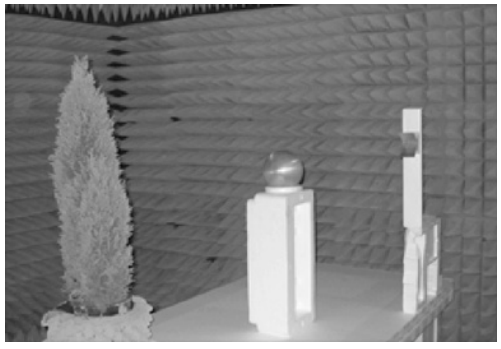

(b) Measurement situation.

**Fig. 8** Actual target decomposition.

sible to find its orientation angle using Eq. (18). A parallel plate waveguide [6] is used in the measurement that exhibits wire-like polarimetric scattering characteristics with enhanced RCS. The estimated angle and actual angle are shown in Fig. 7. They are also in quite good agreement.

### 3.4 Actual Target Decomposition

To see the actual complex object (not necessarily metallic scatterer), we tried to decompose them. Figure 8 shows the measurement situation and the decomposed result. In this case, a tree, a metallic sphere, and a diplane in Table 3 were set along the range direction. Scattering matrices along the range were obtained for this configuration. SAR processing is not available in this case. Using real aperture data, they are decomposed as shown in Fig. 7. The wire component power $P_w$ is dominant for the plant exhibiting randomly oriented angles along the range. The sphere has the single bounce component $P_s$, and the diplane has the double bounce component $P_d$. The algorithm decomposed actual scatterer quite well.

## 4. Discussion

The decomposition scheme is based on the coherent scattering. If the data is not sufficient, the second-order statistics of polarimetric information is not available. In this regard, the coherent decomposition for small number of data was proposed. In the experiment, we tried several matrix averaging along the range cells for the decomposition. This small number of scattering matrix was found to be sufficient for decomposition purpose regardless of data type (i.e., the method can be applied to both real aperture data and SAR data). However, it is necessary to examine the most appropriate number of scattering matrices for this kind of decomposition, because the rank of coherency matrix is 1 for single scattering matrix case [1].

## 5. Conclusion

This paper presented a coherent decomposition scheme of fully polarimetric SAR and real aperture data. The coherent decomposition is applied to a few scattering matrix data. This method can be used for coherent and incoherent data analysis. Based on the scattering matrix data acquired with an FM-CW system, we have demonstrated the decomposition capability. It is shown the scattering mechanisms are well recognized by the scheme including orientation angles of wire target. Since decomposition scheme is based on the coherency matrix with the orthogonal Pauli basis, the decomposed result reflects the scattering mechanisms and the scattering characteristics of targets directly.

#### References

[1] S.R. Cloude and E. Pottier, "A review of target decomposition theorems in radar polarimetry," IEEE Trans. Geosci. Remote Sens., vol.34, no.2, pp.498–518, March 1996.
[2] E. Krogager and Z.H. Czyz, "Properties of the sphere, diplane, helix (target scattering matrix) decomposition," Proc. JIPR-3, pp.106–114, March 1995.
[3] Y. Yamaguchi, Y. Yajima, and H. Yamada, "A four-component decomposition of POLSAR images based on the coherency matrix," IEEE Geosci. Remote Sens. Lett., vol.3, no.3, pp.292–296, July 2006.
[4] Y. Yamaguchi, M. Nakamura, and H. Yamada, "Decomposition of radar target based on the scattering matrix obtained by FM-CW radar," IEICE Trans. Commun., vol.E80-B, no.10, pp.1564–1569, Oct. 1997.
[5] M. Ikarashi, J. Nakamura, K. Aoyama, Y. Yamaguchi, and H. Yamada, "Laboratory measurements by a fully polarimetric FM-CW SAR in the Ku-band," Electronic Proc. PIERS 2006, Tokyo, Aug. 2006.
[6] K. Kitayama, Y. Takayanagi, Y. Yamaguchi, and H. Yamada, "Polarimetric calibration using a corrugated parallel plate target," IEICE Trans. Commun. (Japanese Edition), vol.J81-B-II, no.10, pp.914–921,

Oct. 1998.
[7] Y. Yamaguchi, Radar Polarimetry from Basics to Applications, IEICE, Dec. 2007.

**Jun Nakamura** received the B.E. and M.E. degrees from Niigata University in 2006 and 2008, respectively, in information engineering. He has been engaged in developing a fully polarimetric and interferometric FM-CW radar system with applications to Coherent Change Detection.

**Kazuyasu Aoyama** received the B.E. and M.E. degrees from Niigata University in 2006 and 2008, respectively, in information engineering. He has been engaged in developing a fully polarimetric and real-time FM-CW radar system.

**Muneyuki Ikarashi** received the B.E. and M.E. degrees from Niigata University in 2005 and 2007, respectively, in information engineering. He has been engaged in developing a fully polarimetric FM-CW radar system.

**Yoshio Yamaguchi** received the B.E. degree in electronics engineering from Niigata University in 1976, and the M.E. and Dr.Eng. degrees from Tokyo Institute of Technology in 1978 and 1983, respectively. In 1978, he joined the Faculty of Engineering, Niigata University, where he is a professor. His interests are in the field of radar polarimetry, microwave sensing and imaging. He has served as Chair of IEEE GRSS Japan Chapter (02–03), vice chair (00–01), Chair of URSI-F Japan since 06. He is a Fellow of IEEE and The Electromagnetics Academy.

**Hiroyoshi Yamada** received the B.E., M.E., and Dr.Eng. degree from Hokkaido University, Japan, in 1988, 1990, and 1993, respectively, all in electronic engineering. In 1993, he joined the Faculty of Engineering, Niigata University, where he is a Professor. His interests involve in the field of array signal processing, polarimetric radar interferometry, and high-resolution techniques. He is a member of IEEE.